A new validated mathematical model of the Wnt signaling pathway predicts effective combinational therapy by sFRP and Dkk

Yuri Kogan[*,1], Karin E. Halevi-Tobias[*], Gili Hochman[*], Anna K. Baczmanska[†], Luc Leyns[†], Zvia Agur[*]

[*]Institute for Medical BioMathematics, 10 Hate'ena St., P.O.B. 282, Bene Ataroth 60991, Israel
[†]Laboratory for Cell Genetics, Vrije Universiteit Brussel (VUB), Pleinlaan 2, B-1050 Brussels, Belgium
[1]Corresponding author. Address: Institute for Medical BioMathematics, 10 Hate'ena St., P.O.B. 282, Bene Ataroth 60991, Israel. Tel: 972-3-9734068 / 9733075 Fax: 972-3-9733410, email: yuri@imbm.org

Short title: Validated model of Wnt pathway

Keywords: Wnt pathway, signal transduction, computational modeling, sFRP, Dkk, ODE

Synopsis

The Wnt signaling pathway controls cell proliferation and differentiation, and its deregulation is implicated in different diseases, including cancer. Learning how to manipulate this pathway is of great promise for therapy. We developed a mathematical model, describing the initial sequence of events in the Wnt pathway, from ligands binding down to β-catenin accumulation, and the effects of inhibitors, such as secreted frizzled-related proteins (sFRP) and Dickkopf (Dkk). Model parameters were retrieved from experimental data reported in the literature. The model was retrospectively validated by accurately predicting the effect of Wnt3a and sFRP1 on β-catenin level in two independent published experiments (R^2 between 0.63 and 0.91). Prospective validation was obtained by testing the model's accuracy in predicting the effect of Dkk1 on Wnt-induced β-catenin accumulation ($R^2 \approx 0.94$). Model simulations under different combinations of sFRP1 and Dkk1 predicted a clear synergistic effect of these two inhibitors on β-catenin accumulation, which may point towards a new treatment avenue. Our model allows precise calculation of the effect of inhibitors applied alone or in combination, and provides a flexible framework for identifying potential targets for intervention in the Wnt signaling pathway.

Introduction

The Wnt signaling pathway controls mechanisms that direct cell proliferation, polarity, and fate determination during embryonic development and in tissue homeostasis. Mutations in the Wnt pathway are often linked to different diseases, including cancer [1-2]. Many genes in the Wnt pathway, initially discovered as transiently functioning in development, turned out to be oncogenes and tumour suppressors [3-4]. The special significance of Wnt signaling in stem and progenitor cells implies its role in regulating cancer stem cells (CSCs), which are thought to be associated with relapse, metastasis and drug resistance [5-6].

A significant effort is currently invested worldwide in developing therapeutic agents that function by manipulating the Wnt pathway, in particular, those that may provide a novel approach to limit tumor growth [3, 6-8]. Therapeutic application of regulatory proteins that inhibit the Wnt pathway, such as sFRP, is presently developed for the treatment of cancer [9-11]. Since this pathway is used primarily during embryogenesis and in adults for tissue repair, significant levels of toxicities are not expected [6].

There are at least 19 Wnt ligands and 10 Frizzled receptors, activating at least three intracellular signaling pathways [4, 12-13]. This vast network is influenced by a wide range of regulators, including two main classes of extracellular inhibitors: those directly interacting with Wnt proteins (e.g. sFRP, WIF) and those binding to Wnt receptors or co-receptors (e.g. Dkk binding to LRP) [14-15]. The complexity of the interactions between ligands, antagonists and receptors makes the Wnt signaling amenable to therapeutic intervention at many target points. However, it is not intuitively clear which component of the system will be the best target for therapeutic intervention, and how such intervention should be designed in order to achieve the best clinical outcomes.

Mathematical models based on biological information are effective in improving the understanding of complex signaling pathways and their role in disease control [16]. Such models are simplified to include only the main components of the signaling pathways, yet ensuring that the fundamental properties of the system are retrieved [17]. Theoretical and numerical analysis of the mathematical model may be used to

predict the system behavior under various scenarios, which then can be compared to new experimental data [17]. One example is the MAPK pathway, where mathematical models have led to new insights and predictions [18]. An important test of model validity is its predictive accuracy under a wide range of conditions. As quantitative information on signal transduction pathways is rarely available, most mathematical models of these pathways, while contributing to conceptual understanding, are yet to be substantiated by experimental data.

Among the Wnt-activated pathways, the canonical Wnt pathway is the most critical and best characterized. It regulates the transcriptional co-activator β-catenin, which controls the expression of specific target genes [4]. The dynamical behavior of the intracellular components of this pathway has been studied in detail by a mathematical model, built and parameterized on the basis of experiments in Xenopus extracts [19]. This model was further analyzed [20-21], and extended by adding more pathway-related reactions [22-25]. These models focus on the intracellular steps of the canonical Wnt pathway [26]. However, modeling the initial steps of this pathway, i.e., the binding of extracellular ligands and inhibitors to membrane receptors, is essential for elucidating the potential role of different Wnt signal inhibitors, hopefully paving the way to development of innovative therapeutic interventions. For example, a relatively simple model for the two main signaling pathways, Wnt and Notch, suggesting that exogenous Dkk1 is a potential modulator of stem cell fate decision was verified experimentally in mammary CSCs [27]. However, this model's simplicity, while rendering it analytically tractable, was an impediment to quantitatively evaluating the chemical reactions in these pathways [28].

In this work we developed a detailed mechanistic model for the extracellular and intracellular parts of the canonical Wnt pathway. The predictability of this general model was retrospectively validated by data from independent experiments, testing the effect of Wnt3a and sFRP. We also conducted experiments testing inhibition by Dkk1, which prospectively validated model predictions of this effect. Simulations of the combined effects of sFRP1 and Dkk1 predicted synergism between these inhibitors.

Materials and methods

1. Mathematical model of the Wnt pathway

1a. Basic assumptions and kinetic model

Our model, schematically described in Fig. 1, represents in detail the interactions between Wnt ligand, its inhibitors and cell surface receptors, whereas the intracellular part is represented more generally. The pathway is activated by Wnt ligand binding Frizzled receptor [29-30]. The resulting receptor-ligand complex may recruit an unoccupied LRP receptor and create a ternary complex, consisting of Wnt, Frizzled and LRP [31-33]. The latter transduces the signal inside the cell and interferes with β-catenin destruction cycle [34-35].

The intracellular β-catenin is regulated by a specific destruction complex, including Axin, APC and GSK3β. This complex binds β-catenin, and causes its phosphorylation. Phosphorylated β-catenin dissociates from the destruction complex and is rapidly degraded [4]. Four assumptions of our model are consistent with those in Lee et al [19]: (i) the destruction complex is at equilibrium with its components, so that its total concentration is constant; (ii) upon dissociation from phosphorylated β-catenin, the destruction complex may bind another β-catenin molecule; (iii) β-catenin is produced at constant rate; and (iv) there exists an additional slow degradation path

of β-catenin, independent of the destruction complex. To reduce the model complexity, β-catenin phosphorylation, dissociation from the complex and degradation are represented as a one-step process.

The regulation of β-catenin destruction cycle by Wnt signal is carried out via the intracellular domain of the LRP receptor. When bound into ternary complex with Wnt and Frizzled, LRP receptor binds intracellular Axin [36-37]. For simplicity, our model assumes that the whole destruction complex is bound to the intracellular part of the activated LRP, in line with the above assumption of equilibrium between the complex and its components. We also assume that the binding of the destruction complex to the intracellular domain of LRP is reversible, and upon dissociation, the receptor complex decomposes into its components [38]. The bound destruction complex cannot participate in β-catenin destruction cycle. Hence, high Wnt concentration leads to the formation of active ternary Wnt-Frizzled-LRP complexes, which reduce β-catenin destruction, allowing its accumulation.

The model includes down-regulation of the pathway by sFRP, which competes with Frizzled for Wnt binding [39-40], and Dkk, which binds to LRP and abolishes formation of the ternary complex [15, 41]. The total concentrations of all system components, except for β-catenin, are assumed constant over time of interest.

1b. Model equations

The above description was converted into balance ordinary differential equations (ODEs), assuming well-mixing and law of mass action for all the protein interactions. The model describes the dynamics of 13 state variables, standing for the concentrations of the modeled pathway components by a system of seven ODEs. We close the system by six conservation equations for the total concentrations of Wnt (W_T), destruction complex (C_T), sFRP (S_T) and Dkk (D_T) and for the numbers of Frizzled (F_T) and LRP (L_T) receptors:

$$\dot{S}_W = k_1 SW - k_{-1} S_W$$
$$\dot{L}_D = k_4 DL - k_{-4} L_D$$
$$\dot{F}_W = k_2 FW - k_{-2} F_W - K_{su-in} k_3 LF_W + k_{-3} L_F$$
$$\dot{L}_F = K_{su-in} k_3 LF_W - k_{-3} L_F - k_5 L_F C$$
$$\dot{C}_L = k_5 L_F C - k_{-5} C_L$$
$$\dot{C} = -K_{su-in} k_5 L_F C + K_{su-in} k_{-5} C_L - k_6 CB + k_{-6} C_B$$
$$\dot{B} = k_7 - k_8 B - k_6 CB$$
$$C_B = C_T - C - K_{su-in} C_L$$
$$L = L_T - L_F - C_L - L_D$$
$$F = F_T - F_W - L_F - C_L$$
$$W = W_T - \left(F_W + L_F + C_L\right) \cdot K_{su-ex} - S_W$$
$$S = S_T - S_W$$
$$D = D_T - L_D \cdot K_{su-ex}$$

The state variables represent extracellular free Wnt (W), Frizzled receptors, free (F) and bound to Wnt (F_W), free LRP receptors (L), ternary receptor complexes Frizzled/Wnt/LRP (L_F), intracellular destruction complex, free (C), bound by the

ternary receptor complex (C_L) and bound to β-catenin (C_B), intracellular free β-catenin (B), extracellular sFRP, free (S) and bound to Wnt (S_W), extracellular free Dkk (D) and LRP receptors bound to Dkk (L_D).

Reaction rates are given by the coefficients $k_{\pm i}$, where i is the reaction step index as shown in Fig. 1, and the sign corresponds to the reaction direction. Association reaction rates, k_i, have units of $M^{-1}s^{-1}$, while dissociation rates have units of s^{-1}. Note, that variables related to different cell compartments have different units: intra- and extracellular proteins are measured in molar (M), while free or bound receptors in cell membrane are measured in number per cell, *receptor/cell*. For computing reactions between components measured in different units, we used partition coefficients, $K_{su\text{-}ex}$ and $K_{su\text{-}in}$, translating numbers in cell membrane to extracellular and intracellular concentrations, respectively. These coefficients were determined as follows: $K_{su-ex} = \frac{N_{Cells}}{Av \cdot V_{\exp}}$, $K_{su-in} = \frac{1}{Av \cdot V_{cell}}$, where N_{Cells} is the number of cells, V_{exp} is the experimental volume (both depending on experimental conditions), V_{cell} is the intracellular compartment volume and Av is Avogadro number. For the estimation of $K_{su\text{-}ex}$ we assumed that experimental volume is a well-mixed external compartment. The estimation of $K_{su\text{-}in}$ is based on a similar assumption for intracellular cytoplasmatic volume.

1c. Computer implementation

The model was solved numerically by an ODE solver in MATLAB. Whenever parameters were adjusted, it was performed by repetitive applications of a local search algorithm (*trust region*) in MATLAB, each time with random initial guess for the adjusted parameters within the ranges determined for these parameters (Appendix A); other parameter values were set at literature-based values (see below).

2. Data acquisition from the literature

We employed published experimental data on time course of β-catenin accumulation induced by different Wnt3a concentrations [42], and inhibition of this effect by sFRP at different concentrations [43-44]. These experiments were conducted in L cells, which do not express cadherins, hence the cytoplasmatic β-catenin is free and not bound to the membrane. This makes these data suitable for comparison with our model, which does not include the binding of β-catenin to cadherins.

The measurements of the time course of β-catenin accumulation in L cells, stimulated by different concentrations of Wnt3a were extracted from Fig. 4C,D in [42]. These results are averages of two independent experiments, each carried out in quadruplicate. The sampled data were represented as a matrix E, where $E_{i,j}$ is the β-catenin fluorescence intensity at time t_i under concentration W_j of Wnt3a, $1 \le i,j \le 10$. We also constructed a corresponding matrix M of weights, $M_{i,j} \in \{0,1,2\}$ being the number of values available from graphical sampling of measurement $E_{i,j}$.

Accumulation of β-catenin after a fixed period of stimulation by different concentrations of Wnt3a, as well as inhibition of Wnt3a effect by different concentrations of sFRP, were obtained from our previous work [44] and from Figs. 1C and 2 in [43].

For all the published measurements we extracted average values. We also report s.e.m. estimations, whenever available from the relevant publication source.

3. Parameter evaluation

The initial estimation of parameter values and ranges was based on various literature sources (Appendix A). Then data extracted from [42] were used to fine-tune the model for Wnt effect. This was done in two steps: (1) adjustment of alternative subsets of model parameters to fit part of the experimental data (denoted "partial training set") and (2) selection of the best-predictive parameter set, using the whole experimental data set.

The partial training set was formed by selecting three of the ten experimentally tested Wnt3a doses (0, 12.5 and 400 *ng/ml*). All the time course measurements of β-catenin accumulation for these doses were included in the partial training set $\{E_{i,j} | i=1,\ldots,10; j \in \{1,5,10\}\}$.

At the first step, we considered several alternative choices of a subset of adjusted parameters (see Appendix B), focusing on those parameters for which our initial estimation based on literature was assumed to be less reliable. Each subset of model parameters was adjusted by fitting model predictions to the partial training set, while other parameters were set at their initially estimated values reported in Appendix A.

Given the vector v of the values of adjusted parameters, the model was simulated as follows. We set $S_T = 0$ and $D_T = 0$, since in [42] no inhibitors were added, and used the reported experiment volume and cell number. For each Wnt3a concentration, W_j, the model was initiated with free Wnt concentration (and W_T) equal to W_j, and other variables at their unique steady-state values assumed in absence of Wnt. The model was numerically integrated from time $t=0$ to $t=t_{10}=35$ *hours*. To compare the simulations to the experimental results, we interpreted the latter in terms of the model variables. We assumed that the reported fluorescence measurements were in direct proportion to the concentration of total β-catenin, with proportion coefficient λ. Model predictions for β-catenin accumulation at time t_i were computed as $P_{i,j}(v)=\lambda(B(t_i)+C_B(t_i))$, for a given Wnt3a concentration W_j, and for parameters values v. The value of λ was included in all subsets of adjusted parameters.

For each choice of a subset of adjusted parameters, the values were determined by minimizing the Goal Function (*GF*), computed by comparing simulation results to the partial training set data. We defined *GF* as a sum of squares of differences between model-predicted and observed measurements, with weights taken from matrix *M*.

$$GF(v) = \sum_{j \in J} \sum_{i=1}^{10} M_{i,j} \left(E_{i,j} - P_{i,j} \right)^2 ,$$

where $J=\{1,5,10\}$ is the partial training set, $E_{i,j}$ are the experimental data points and $P_{i,j}$ are the corresponding model predictions under the parameter set v. The values of the adjusted parameters that minimize *GF* were found using the search algorithm with initial guesses randomly chosen within the relevant parameter ranges (reported in Appendix A).

Subsequently, in order to select the best-predictive parameter set among those resulted from the first step, we compared the model predictions generated by these different parameter sets to the whole data extracted from [42]. For each parameter set, the whole experiment was simulated, and the resulting values of $P_{i,j}$ were compared to the data. We used several statistical tests for correlation between observed and predicted values (see Appendix B). For example, we calculated the coefficient of determination, R^2, defined as $R^2 = 1 - \frac{SS_{err}}{SS_{tot}}$, where SS_{err} is the sum of squares of differences between model-predicted and observed measurements, with weights taken

from the matrix M, $SS_{err} = \sum_{j=1}^{10}\sum_{i=1}^{10} M_{i,j}\left(E_{i,j} - P_{i,j}\right)^2$, and SS_{tot} is the total sum of squares of the data, proportional to the sample variance, with weights taken from the matrix M, $SS_{tot} = \sum_{j=1}^{10}\sum_{i=1}^{10} M_{i,j}\left(E_{i,j} - \overline{E}\right)^2$. Here, $\overline{E} = \frac{\sum_{j=1}^{10}\sum_{i=1}^{10} M_{i,j}E_{i,j}}{\sum_{j=1}^{10}\sum_{i=1}^{10} M_{i,j}}$ is the weighted mean of the observed data. This definition of R^2 implies that $R^2 \leq 1$ and for better fit, the result is closer to 1. This index was used also for comparing model predictions to experimental data during model validation.

The selected best-predictive parameter set (Table 1) was used for further model simulations.

4. Experiments testing Dkk1 inhibition of Wnt-induced β-catenin accumulation

Proteins. Recombinant mouse Wnt3a and Dkk1 were purchased from R&D systems (Minneapolis, MN).

Assaying Wnt3a signaling by measuring β-catenin accumulation. The experiments were conducted in the same conditions as previously reported [44]. Mouse fibroblasts (L cells) were plated on 24-well plates, 250,000 cells/well, and grown overnight. They were incubated for 30 minutes in a serum-free medium, and, then, for another 30 minutes, with or without Dkk1. Thereafter, Wnt3a (0.5 *nM* final concentration) was added. Two hours later the cells were lysed and analyzed by Western blot.

β-catenin protein was detected by Western blotting with anti-β-catenin mouse monoclonal antibody (BD Transduction Laboratories), and measured in BioRad ChemiDoc XRS. The membranes were re-blotted with mouse anti-β-actin antibody (Sigma). Numerical data of band intensity were obtained using Quantity One X software. β-catenin band intensities were standardized respective to β-actin band intensities. The densitometric intensity of experimental β-catenin bands was corrected by subtracting the negative control. These data were normalized to a scale where the relative densitometric value of β-catenin accumulation, induced by 0.5 *nM* of Wnt3a, two hours after treatment was set at 100%. The results were expressed as the means of 3 experiments ± s.e.m., analyzed by ANOVA followed by a post-hoc multiple comparison test (using SPSS 16.0 software).

5. Model validation

5a. Predicting the effect of Wnt3a and sFRP

From two independent experimental works [43-44], we extracted data on the inhibitory effect of sFRP on Wnt-induced β-catenin accumulation (see section 2). Both works report accumulation of β-catenin by several different concentrations of Wnt3a after three [43] or two hours [44]. In order to compare the results of the two experiments with model predictions, we scaled each one of them, separately, to the results of the previously analyzed experiment [42], by linear units scaling. The proportion coefficient between the measurement units of the experiment in [44] to those of [42] was found by minimizing the sum of square of differences between β-catenin measurements in the two experiments at t=2 hours, for the same concentrations of Wnt3a. This coefficient is equal to the proportion between the

corresponding values of parameter λ (defined in section 3). Similar scaling was performed for the data from [43], using the average between measurements at t=2 and t=4 hours in [42] for each Wnt3a concentration, since no measurements at t=3 hours were available there. The above proportion coefficients were used to compute the values of λ for simulating each of these experiments.

To simulate the experiments testing Wnt3a effect, we used the same initial conditions as in the previously described simulation, and experiment volume and cell number reported for each experiment. The concentration of Wnt3a was set to 0.5 *nM* and 2.5 *nM*, as reported for the experiments [44] and [43], respectively. The model was simulated over two or three hours, corresponding to the duration of the respective experiment, and total computed β-catenin accumulation was compared to the experimental results.

Further, the model was used to predict the inhibition effect of sFRP1 and sFRP2. To this end, we simulated the sFRP inhibition experiments, with S_T values ranging from 0 to 16 and from 0 to 500 *nM*, covering the range of experimental sFRP concentrations in [44] and [43], respectively. The inhibition of β-catenin accumulation was computed as the ratio between total Wnt-induced β-catenin accumulation, with and without sFRP. For this computation, the base level of β-catenin, i.e., that obtained for W_T=S_T=0, was subtracted from both values in the ratio, as done with the experimental results.

An additional adjustment of the rate parameters for sFRP2-Wnt binding was performed using the results of sFRP2 inhibition experiment [43]. This was done fixing all the other model parameters and using the search algorithm to determine the best-fit values for k_1 and k_{-1}, within the range of one order of magnitude from the values reported in [44].

5b. Model validation using experimental results of inhibition by Dkk1

We used the model to predict Dkk1 inhibition of Wnt-induced β-catenin accumulation. The initial values were defined as previously, and experimental volume and cell number were set in accordance with section 4. The values of D_T ranged from 0 to 10 *nM*. The inhibition was computed as the ratio between total β-catenin levels with and without Dkk1, after 2.5 hours. Baseline β-catenin level was subtracted from both values.

6. Predicting the combined effect of sFRP and Dkk

We simulated the effect of sFRP1 and Dkk1 combination on Wnt induced β-catenin accumulation, using the experimental volume and cell numbers as in section 4. We checked different Wnt3a concentrations, in the range of 0.05 to 5 *nM*. For each Wnt3a dose, we simulated the effects of adding different combinations of sFRP1 and Dkk1 concentrations in the experimentally relevant concentrations range (for Dkk1 0–40 *nM* and for sFRP1 0–300 *nM*). These results were used to examine whether the combined effect of sFRP1 and Dkk1 is additive or synergistic. For this purpose, we created isoboles [45] – curves that represent a set of sFRP1 and Dkk1 dose pairs that give a specified effect, in the presence of a given Wnt3a concentration. Such isoboles were constructed for several levels of β-catenin inhibition and different Wnt3a concentrations. The ratio between sFRP1 and Dkk1 doses that separately achieve the same effect is termed potency ratio. We determined a maximally synergistic combination as the point on the isobole that minimizes the sum of sFRP1 and Dkk1

doses, scaled by the potency ratio. A synergistic effect would be most significant at this point.

Results

1. Model calibration

The mathematical model for the canonical Wnt pathway was constructed on the basis of published biological knowledge (see Fig.1 and section 1 in Materials and Methods). Model parameters were initially estimated based on various published experimental sources (see Appendix A). Subsequently, the model was fine-tuned using data of time course of β-catenin accumulation under various Wnt3a concentrations [42]. For details of model fine-tuning see Materials and Methods section 3. We found that adjusting as few as 4 parameters to a subset of the data, comprising measurements for 3 Wnt3a concentrations (0, 12.5 and 400 *ng/ml*), was sufficient to obtain a good fit to data for all other Wnt3a concentrations (Fig. 2) with unbiased residual distribution (Fig. 3). The adjustment of these 4 parameters resulted in the final set of parameters of our model (Table 1). Predictions generated using this parameter set, when compared to the complete data set [42], had mean absolute error of 0.025 and coefficient of determination $R^2 \approx 0.965$. These results demonstrate that our model accurately predicts the time course of Wnt-induced β-catenin accumulation. Hence, the obtained set of equations and parameters constitutes our general model of the canonical Wnt pathway.

2. Model validation by independent experiments

2a. Validation by predicting the effect of Wnt3a

To study the predictive ability of our model by the results of independent experiments, we employed data from two additional studies [43-44], which had tested the effect of Wnt3a on β-catenin accumulation. Our model predicted the results of these two experiments (Fig. 4), with R^2 values of 0.626 for experiments, that had employed Western blot [44], and 0.908 for experiments, that used ELISA as an assay [43]. Comparing between the results of these experiments and those serving for fine-tuning the model [42], one may observe a close agreement between data in the two ELISA-based experiments, (Fig. 4B), and slightly lower agreement between experiments using two different assays (Fig. 4A). In spite of the small disagreement between results from different experimental assays, the predictive accuracy of our model demonstrates its general applicability.

2b. Validation by predicting sFRP inhibitory effect

Our next step was to validate the model ability to predict the effect of Wnt pathway inhibitors sFRP1 and sFRP2, as reported in two independent studies [43-44].

First, we simulated the model to predict the inhibitory effect of sFRP1. Fig. 5 shows that our model accurately predicts the sFRP1 effect found in both experiments. The R^2 values for predicted vs. observed results are 0.893 and 0.911 for the experiments shown in Fig. 5A and Fig. 5B, respectively.

Next we used our model to predict the effect of sFRP2. Here the prediction accuracy was lower: $R^2 \approx 0.507$ (Fig. 6A); $R^2 \approx -0.65$ (Fig. 6B, solid black line). In the latter case, the model clearly underestimated the experimental effect, as reflected by the negative coefficient of determination. However, this experiment [43] was conducted with chicken sFRP2, while the binding coefficients used for model simulation were estimated for mouse sFRP2 [44].

To check the possibility that binding rates of chicken sFRP2 differ from those reported for mouse sFRP2, we fine-tuned the rate parameters for sFRP2-Wnt3a binding by fitting to the experiment results in [43], without changing any other parameter. The results (Fig. 6B, dashed blue line) show that increasing binding rate to $k_1 \approx 8.89 \cdot 10^5 M^{-1} s^{-1}$ and decreasing dissociation rate to $k_{-1} \approx 7.8 \cdot 10^{-5} s^{-1}$ (both contributing to decrease in dissociation constant) render the model predictions of the experimental observations accurate ($R^2 \approx 0.914$).

2c. Prospective validation by experiments evaluating Dkk1 inhibitory effect

We prospectively validated the ability of our model to predict the effect of Dkk1. The model predicted inhibition of β-catenin accumulation by low Dkk1 concentrations ($IC_{50} \approx 2.4$ nM. see Fig. 7A, black line). To test model predictions, we performed experiments in L cells. The experimental results show that Dkk1 inhibited Wnt3a-induced β-catenin accumulation in a dose-dependent manner with $IC_{50} \approx 3.2$ *nM*, as shown in Fig. 7. Overall, the predictions of the model for Dkk1 effect were validated by the experimental results ($R^2 \approx 0.944$), verifying its quantitative accuracy.

3. Model predictions of the combined effect of sFRP and Dkk

Our next goal was to use the validated model for studying the combined quantitative effect of both inhibitors, sFRP and Dkk, when applied simultaneously with Wnt, at various concentrations. Figs 8A,B show examples of simulation results under 0.5 and 5 *nM* Wnt3a, respectively. It can be seen that the effect of each inhibitor in the combination increased with its concentration, and Dkk1 had a stronger effect than sFRP1 (also due to lower K_d).

We analyzed the combined effect of the two inhibitors. Figs 8C,D show isoboles (see Materials and Methods, section 6) produced by model simulations. Each curve represents different combinations of sFRP1 and Dkk1 that inhibit β-catenin accumulation to a fixed level, in the presence of a given Wnt3a concentration. Isoboles for β-catenin inhibition to 10% of its maximal level are shown in Fig. 8C, each curve corresponding to a different Wnt3a dose. Conversely, in Fig. 8D, each curve represents β-catenin inhibition to a different fixed level, in the presence of 0.5 *nM* Wnt3a. The convex form of the curves in Figs 8C,D suggests a synergistic effect of the two inhibitors in all the Dkk1 and sFRP1 concentrations tested, i.e. the effect of the combination is higher than additive, since an additive effect would have yielded linear curves. Hence, lower concentrations of Dkk1 and sFRP1 can be combined to achieve significant inhibition of β-catenin. We also simulated application of the same concentration combinations, varying each of the model parameter values up to +/- 50%, and observed similar synergistic behavior under all of the Dkk1, sFRP1 and Wnt3a concentrations tested (data not shown). This result implies that the observed synergistic effect is robust, probably imposed by the pathway structure.

Table 2 shows different combinations of sFRP1 and Dkk1 that are expected to inhibit Wnt-induced β-catenin accumulation to the same level, in the presence of a fixed Wnt3a concentration; each row contains values of five points on one of the isoboles shown in Figs 8C,D. The synergistic effect of Dkk1 and sFRP1 is clearly seen in Table 2 by comparing predicted concentrations of combined sFRP1 and Dkk1 (columns ***b***, ***c*** and ***d***) to the concentrations needed to achieve the same effect by each inhibitor alone (columns ***a*** and ***e***).

Column ***c*** shows the maximally synergistic simulated combination of sFRP1 and Dkk1, i.e. the point where the synergism is most noticeable (see Materials and

Methods, section 6). In presence of 0.5 *nM* Wnt3a, the maximally synergistic combination that inhibits β-catenin accumulation to 10% suggests a ratio of about 3.6:1 between sFRP1 and Dkk1. This ratio is increasing when higher doses of Wnt3a are applied (see rightmost column in Table 2). Interestingly, this ratio is approximately the same as the potency ratio between the concentrations of sFRP1 and Dkk1 needed to achieve the same effect when added alone (compare last two columns in Table 2).

Discussion

Mathematical modeling enables to better understand complex biological systems and may reveal improved treatment strategies. We used this approach to investigate the Wnt canonical pathway and provide a new mechanistic framework for this pathway, which can serve as a platform for discovering new anti-cancer treatments. Our model is new in detailing the sequence of events occurring along the pathway, from the ligands and inhibitors binding the membranal and extracellular components of the pathway to β-catenin regulation. This allows exploring the quantitative effects of different extracellular pathway inhibitors, including therapeutic agents. This feature of the model distinguishes it from previously published mathematical models of the Wnt pathway, whose focus is set on intracellular components, as recently reviewed [26]. The parameters for our model were evaluated using published experimental studies.

Our model was validated using several independent experimental studies. It accurately predicted experimental results of the effects of Wnt and sFRP, obtained in different laboratories, by different assays, and across a wide range of concentrations [42-44]. In addition, model predictions concerning Dkk1 effect were prospectively validated experimentally. Altogether, the model predictions were in good agreement with most of the experimental results, namely those of Wnt-induced β-catenin accumulation (Fig. 4) and the effect of the inhibitors, sFRP1 and Dkk1 (Figs 5, 7). Note, that binding rates for these inhibitors, which are most influential on model predictions, were already fixed from literature in the initial stage of parameter estimation. This demonstrates that our model is able to quantitatively predict the effects of inhibitors of the Wnt pathway.

For the effect of sFRP2 on Wnt-induced β-catenin accumulation, the model was less accurate (Fig. 6). This can be explained by imprecise estimation of the rates of sFRP2 binding to Wnt3a. In one of the experiments [43] chicken sFRP2 was used, while the reaction rates assumed in our model were taken from mouse sFRP2 experiments [44]. Fitting the sFRP2-Wnt3a reaction rates to experimental results with chicken sFRP2 led to significant improvement in predictions accuracy (Fig. 6B). This demonstrates the applicability of our model for determining unknown specific parameters of Wnt pathway inhibitors (including potential drugs), when experimental data of their effect are available.

The Dkk1 dose-response relationship in our experiment varied from that recently found by others, difference being two orders of magnitude in IC_{50} [46]. The reason underlying this discrepancy may be that in the latter study, the constant of dissociation (K_D) between Dkk1 and LRP was significantly higher than the previously reported K_D values [15, 41]. This difference in Dkk1 binding coefficient may result from different protein expression systems and purification procedures.

Despite the abundance of published research on the canonical Wnt pathway, there are still parts of this pathway whose underlying mechanism is not clear. For example, our modeling hypothesis that Wnt-Frizzled complex is created and subsequently binds

to LRP is consistent with previous experimental results, but to the best of our knowledge had not been explicitly stated before. Experimental validation of our model lends support to the basic biological assumptions laid at its foundation, including this hypothesis.

Our general mechanistic model characterizes the canonical Wnt signaling pathway for different biological systems, and it is not tailored to a specific experimental setup. Hence, the model can be used to forecast results of various experiments, by input of a few parameters that characterize the specific experiment (e.g. cell number). New biological information, such as the binding affinities between specific Wnt ligands, their receptors and different inhibitors may also be easily incorporated into the model.

Since our model explicitly describes the extracellular part of the Wnt pathway, it can predict effects of various drugs that intervene in Wnt ligand-receptors interactions or act on the modeled intracellular components. Therefore, it provides a flexible framework for planning an intervention in the Wnt signaling pathway and can be also used to predict the combined effect of drugs acting on both intra- and extracellular pathway components.

To demonstrate an application for quantitatively predicting the combined effect of two inhibitors, we have simulated the combined effect of sFRP1 and Dkk1 on Wnt-induced β-catenin accumulation and found it synergistic. We have determined several possible combinations of sFRP1 and Dkk1 that would give similar inhibition effect, including the combination that most effectively demonstrates the synergism. This newly predicted synergism, which was not previously explored, should be experimentally verified. This may lead to the development of a new treatment modality for cancer and other diseases, namely, a combination of Wnt pathway inhibitors which are active through complementary mechanisms, like Dkk and sFRP.

In conclusion, our validated mathematical model of the initial stages of the canonical Wnt pathway is a useful tool for predicting the effects of different pathway inhibitors, alone or in combination. Our model provides a general framework for analysis of experimental data and systemic approach to investigating the Wnt pathway. Currently, we examine its use for studying the effects of different cancer-related mutations in the Wnt pathway and predicting effects of different pathway inhibitors or drugs on these mutants. The application of our model as a tool for testing the effect of possible therapeutic interventions should be further studied.

Appendix A: Initial parameter estimation

Here we describe the estimation procedure for the model parameters, from published sources. To allow model fine-tuning by adjusting some of the parameters, we also defined a range for every parameter. A range of one order of magnitude below and above the literature-based value was assumed, unless specified otherwise.

Wnt-sFRP reaction rates, k_1 and k_{-1}: We used the coefficients measured by [44] for sFRP1: $k_1 \approx 4.33 \cdot 10^4 M^{-1}s^{-1}$, $k_{-1} \approx 4.86 \cdot 10^{-4} s^{-1}$ and for sFRP2: $k_1 \approx 11.4 \cdot 10^4 M^{-1}s^{-1}$, $k_{-1} \approx 4.63 \cdot 10^{-4} s^{-1}$. We have neglected the secondary binding reaction rate reported there, due to much higher values of the dissociation rate and constant.

Wnt-Frizzled reaction rates, k_2 and k_{-2}: No direct measurements for this reaction were found. Since the extracellular domains of Frizzled receptors and sFRP proteins have similar structures [47] and binding affinities between Wnt and Frizzled [29, 48] are comparable to those between Wnt and sFRP [44], we have assumed the rates to be the mean of the values, used for sFRP1 and sFRP2: $k_2 \approx 7.9 \cdot 10^4 M^{-1}s^{-1}$, $k_{-2} \approx 4.7 \cdot 10^{-4} s^{-1}$.

Wnt/Frizzled-LRP reaction rates, k_3 and k_{-3}: We could not retrieve from literature the reaction rates for these membrane receptors. For dimerization of a different type of receptors (EGFR), values of $0.01nM^{-1}s^{-1}$ and $0.1s^{-1}$ related to the cytoplasmatic volume were reported [49]. We adopted this estimation as an initial guess. Clearly, the difference between receptor types may lead to significant discrepancy in reaction rates. Therefore, we defined wide ranges for these parameters: $10^4M^{-1}s^{-1}$ to $10^{10}M^{-1}s^{-1}$ for k_3 and $0.001s^{-1}$ to $10s^{-1}$ for k_{-3}.

Dkk-LRP reaction rates, k_4 and k_{-4}: These rates were estimated using the data of Dkk1 binding by LRP6 receptors of NIH3T3 cells [41]. Predictions of a simple binding model (which can be obtained from our model by fixing $W_T=F_T=S_T=0$) were fitted to the time course and steady state data reported there, yielding $k_4\approx1.03\cdot10^6M^{-1}s^{-1}$, $k_{-4}\approx5.05\cdot10^{-4}s^{-1}$ (this gives dissociation constant $K_{D4}\approx0.49nM$ for Dkk1-LRP binding).

Ternary complex-Destruction complex reaction rates, k_5 and k_{-5}: This reaction is the first intracellular signal trigger in our model, and therefore, plays a role similar to that of Dsh_a in Lee-Heinrich model [19]. We took the value reported for the Dsh_a-mediated initiation of the release of GSK3β from the destruction complex [19] to represent the association rate, $k_5\approx5\cdot10^7M^{-1}s^{-1}$, and used a wider range for this parameter, 10^4 to $10^{11}M^{-1}s^{-1}$. The value of k_{-5} is expected to be low, corresponding to the finding that a time-delay of three hours precedes LRP receptors reappearance after internalization [38]. Thus, we set the value $k_{-5}\approx10^{-4}s^{-1}$.

Destruction complex-β-catenin reaction rates, k_6 and k_{-6}: As explained in Materials and Methods section 1a, this step lumps together several successive reactions in β-catenin destruction pathway, namely binding of β-catenin to destruction complex, its phosphorylation, release of phosphorylated β-catenin and its subsequent degradation. The three latter processes are assumed to be governed by the rate of β-catenin release from the complex, k_{-6}. The rates of phosphorylation and dissociation were previously estimated to be both equal to $210min^{-1}$ [19]. We assumed a half of this value for the overall rate of the specific destruction, obtaining $k_{-6}\approx1.75s^{-1}$. The dissociation constant for the destruction complex and β-catenin is estimated to be $120nM$ [19], which can be used to estimate $k_6\approx1.5\cdot10^7M^{-1}s^{-1}$. Both these estimations may be erred, due to differences in β-catenin destruction loop in our model compared to Lee-Heinrich model [19]. Therefore, we chose large ranges: 10^3 to $10^{10}M^{-1}s^{-1}$ for k_6, and 0.01 to $100s^{-1}$ for k_{-6}.

Free β-catenin production and destruction rates, k_7 and k_8: These were adopted from [19]: $k_7\approx7\cdot10^{-12}Ms^{-1}$ and $k_8\approx4.2\cdot10^{-6}s^{-1}$.

Total concentration of destruction complex, C_T: We assumed that it is close to the total concentration of Axin, $C_T\approx0.02nM$, the lowest among the concentrations of proteins involved in the complex [19]. We have assumed the range of $0.001nM$ to $100nM$, the upper bound being the total concentration of APC reported in [19].

Total number of LRP receptors per cell, L_T: This number is estimated between 2500 and 5000 for NIH3T3 cells [41]. We assumed its value is $L_T\approx4000$ *receptor/cell*.

Total number of Frizzled receptors per cell, F_T: Lacking literature information, we assumed $F_T\approx4000$ *receptor/cell*, similarly to our assumption about LRP receptors. However, we used a wider range for this parameter, between 10 to $5\cdot10^5$ *receptor/cell*.

Cell volume, V_{cell} was estimated as cytoplasmatic 70% of an L cell volume reported in [50].

The parameters W_T, D_T, S_T, N_{cell} and V_{exp}, were evaluated separately for each experiment, in accordance with the specific experimental setup.

Appendix B: Model calibration

Parameter adjustment was performed for several choices of parameter subsets. The considered subsets included sets of four to seven parameters, e.g., $\{F_0, k_3, k_6, \lambda\}$,$\{k_3, k_5, k_6, \lambda\}$, $\{F_0, k_3, k_{-5}, k_6, \lambda\}$, $\{F_0, F_C, k_3, k_{-5}, k_6, k_{-6}, \lambda\}$.

The statistical tests used for evaluating the correlation between model-predicted and observed experimental values were:

(i) Mean residual between the simulation results and the experimental data points;
(ii) Average of the square of absolute and relative error per data point;
(iii) The absolute value of absolute and relative error per data point;
(iv) Linear regression for predicted vs. observed data points;
(v) Linear regression, forcing intersection with y-axis to 0;
(vi) Coefficient of determination, R^2 (defined in Materials and Methods section 3).

For tests (i)-(iii) smaller scores indicate better prediction; in test (iv) better prediction should give the intersection closer to zero and the slope and correlation coefficient closer to 1; in test (v) both slope and correlation coefficient should be closer to 1; in test (vi) R^2 should be closer to 1. When calculating average relative error in (ii) and (iii), the experimental points with values less than 0.005 (which is <1% of the maximal experimental result) were excluded from the data set, to prevent bias.

Funding

This work was partly supported by grant #012930 from the NEST FP6 program and by the Chai Foundation.

References

1 Giles, R. H., van Es, J. H. and Clevers, H. (2003) Caught up in a wnt storm: Wnt signaling in cancer. Biochim Biophys Acta. 1653, 1-24

2 Ilyas, M. (2005) Wnt signalling and the mechanistic basis of tumour development. J Pathol. 205, 130-144

3 Klaus, A. and Birchmeier, W. (2008) Wnt signalling and its impact on development and cancer. Nat Rev Cancer. 8, 387-398

4 MacDonald, B. T., Tamai, K. and He, X. (2009) Wnt/beta-catenin signaling: Components, mechanisms, and diseases. Dev Cell. 17, 9-26

5 Massard, C., Deutsch, E. and Soria, J. C. (2006) Tumour stem cell-targeted treatment: Elimination or differentiation. Ann Oncol. 17, 1620-1624

6 Takebe, N. and Ivy, S. P. (2010) Controversies in cancer stem cells: Targeting embryonic signaling pathways. Clin Cancer Res. 16, 3106-3112

7 Barker, N. and Clevers, H. (2006) Mining the wnt pathway for cancer therapeutics. Nat Rev Drug Discov. 5, 997-1014

8 Takahashi-Yanaga, F. and Kahn, M. (2010) Targeting wnt signaling: Can we safely eradicate cancer stem cells? Clin Cancer Res. 16, 3153-3162

9 Chung, M. T., Lai, H. C., Sytwu, H. K., Yan, M. D., Shih, Y. L., Chang, C. C., Yu, M. H., Liu, H. S., Chu, D. W. and Lin, Y. W. (2009) Sfrp1 and sfrp2 suppress the transformation and invasion abilities of cervical cancer cells through wnt signal pathway. Gynecol Oncol. 112, 646-653

10 DeAlmeida, V. I., Miao, L., Ernst, J. A., Koeppen, H., Polakis, P. and Rubinfeld, B. (2007) The soluble wnt receptor frizzled8crd-hfc inhibits the growth of teratocarcinomas in vivo. Cancer Res. 67, 5371-5379

11 Matsuda, Y., Schlange, T., Oakeley, E. J., Boulay, A. and Hynes, N. E. (2009) Wnt signaling enhances breast cancer cell motility and blockade of the wnt pathway by sfrp1 suppresses mda-mb-231 xenograft growth. Breast Cancer Res. 11, R32
12 Kestler, H. A. and Kuhl, M. (2008) From individual wnt pathways towards a wnt signalling network. Philos Trans R Soc Lond B Biol Sci. 363, 1333-1347
13 Kikuchi, A., Yamamoto, H. and Kishida, S. (2007) Multiplicity of the interactions of wnt proteins and their receptors. Cell Signal. 19, 659-671
14 Bovolenta, P., Esteve, P., Ruiz, J. M., Cisneros, E. and Lopez-Rios, J. (2008) Beyond wnt inhibition: New functions of secreted frizzled-related proteins in development and disease. J Cell Sci. 121, 737-746
15 Semenov, M. V., Tamai, K., Brott, B. K., Kuhl, M., Sokol, S. and He, X. (2001) Head inducer dickkopf-1 is a ligand for wnt coreceptor lrp6. Curr Biol. 11, 951-961
16 Ventura, A. C., Jackson, T. L. and Merajver, S. D. (2009) On the role of cell signaling models in cancer research. Cancer Res. 69, 400-402
17 Klipp, E. and Liebermeister, W. (2006) Mathematical modeling of intracellular signaling pathways. BMC Neurosci. 7 Suppl 1, S10
18 Orton, R. J., Sturm, O. E., Vyshemirsky, V., Calder, M., Gilbert, D. R. and Kolch, W. (2005) Computational modelling of the receptor-tyrosine-kinase-activated mapk pathway. Biochem J. 392, 249-261
19 Lee, E., Salic, A., Kruger, R., Heinrich, R. and Kirschner, M. W. (2003) The roles of apc and axin derived from experimental and theoretical analysis of the wnt pathway. PLoS Biol. 1, E10
20 Kruger, R. and Heinrich, R. (2004) Model reduction and analysis of robustness for the wnt/beta-catenin signal transduction pathway. Genome Inform. 15, 138-148
21 Mirams, G. R., Byrne, H. M. and King, J. R. (2009) A multiple timescale analysis of a mathematical model of the wnt/beta-catenin signalling pathway. J Math Biol. 60, 131-160
22 Cho, K. H., Baek, S. and Sung, M. H. (2006) Wnt pathway mutations selected by optimal beta-catenin signaling for tumorigenesis. FEBS Lett. 580, 3665-3670
23 Kim, D., Rath, O., Kolch, W. and Cho, K. H. (2007) A hidden oncogenic positive feedback loop caused by crosstalk between wnt and erk pathways. Oncogene. 26, 4571-4579
24 Wawra, C., Kuhl, M. and Kestler, H. A. (2007) Extended analyses of the wnt/beta-catenin pathway: Robustness and oscillatory behaviour. FEBS Lett. 581, 4043-4048
25 Sun, Y. C. (2009) Examination of effects of gsk3beta phosphorylation, beta-catenin phosphorylation, and beta-catenin degradation on kinetics of wnt signaling pathway using computational method. Theor Biol Med Model. 6, 13
26 Kofahl, B. and Wolf, J. (2010) Mathematical modelling of wnt/beta-catenin signalling. Biochem Soc Trans. 38, 1281-1285
27 Agur, Z., Kirnasovsky, O. U., Vasserman, G., Tencer-Hershkowicz, L., Kogan, Y., Harrison, H., Lamb, R. and Clarke, R. B. (2011) Dickkopf1 regulates fate decision and drives breast cancer stem cells to differentiation: An experimentally supported mathematical model. PLoS One. 6, e24225
28 Kirnasovsky, O. U., Kogan, Y. and Agur, Z. (2008) Analysis of a mathematical model for the molecular mechanism of fate decision in mammary stem cells. Math. Model. Nat. Phenom. 3, 78-89

29 Hsieh, J. C., Rattner, A., Smallwood, P. M. and Nathans, J. (1999) Biochemical characterization of wnt-frizzled interactions using a soluble, biologically active vertebrate wnt protein. Proc Natl Acad Sci U S A. 96, 3546-3551
30 Wu, C. H. and Nusse, R. (2002) Ligand receptor interactions in the wnt signaling pathway in drosophila. J Biol Chem. 277, 41762-41769
31 Cong, F., Schweizer, L. and Varmus, H. (2004) Wnt signals across the plasma membrane to activate the beta-catenin pathway by forming oligomers containing its receptors, frizzled and lrp. Development. 131, 5103-5115
32 Schweizer, L. and Varmus, H. (2003) Wnt/wingless signaling through beta-catenin requires the function of both lrp/arrow and frizzled classes of receptors. BMC Cell Biol. 4, 4
33 Tamai, K., Semenov, M., Kato, Y., Spokony, R., Liu, C., Katsuyama, Y., Hess, F., Saint-Jeannet, J. P. and He, X. (2000) Ldl-receptor-related proteins in wnt signal transduction. Nature. 407, 530-535
34 Cadigan, K. M. and Liu, Y. I. (2006) Wnt signaling: Complexity at the surface. J Cell Sci. 119, 395-402
35 Zeng, X., Tamai, K., Doble, B., Li, S., Huang, H., Habas, R., Okamura, H., Woodgett, J. and He, X. (2005) A dual-kinase mechanism for wnt co-receptor phosphorylation and activation. Nature. 438, 873-877
36 Mao, J., Wang, J., Liu, B., Pan, W., Farr, G. H., 3rd, Flynn, C., Yuan, H., Takada, S., Kimelman, D., Li, L. and Wu, D. (2001) Low-density lipoprotein receptor-related protein-5 binds to axin and regulates the canonical wnt signaling pathway. Mol Cell. 7, 801-809
37 Tamai, K., Zeng, X., Liu, C., Zhang, X., Harada, Y., Chang, Z. and He, X. (2004) A mechanism for wnt coreceptor activation. Mol Cell. 13, 149-156
38 Khan, Z., Vijayakumar, S., de la Torre, T. V., Rotolo, S. and Bafico, A. (2007) Analysis of endogenous lrp6 function reveals a novel feedback mechanism by which wnt negatively regulates its receptor. Mol Cell Biol. 27, 7291-7301
39 Leyns, L., Bouwmeester, T., Kim, S. H., Piccolo, S. and De Robertis, E. M. (1997) Frzb-1 is a secreted antagonist of wnt signaling expressed in the spemann organizer. Cell. 88, 747-756
40 Uren, A., Reichsman, F., Anest, V., Taylor, W. G., Muraiso, K., Bottaro, D. P., Cumberledge, S. and Rubin, J. S. (2000) Secreted frizzled-related protein-1 binds directly to wingless and is a biphasic modulator of wnt signaling. J Biol Chem. 275, 4374-4382
41 Bafico, A., Liu, G., Yaniv, A., Gazit, A. and Aaronson, S. A. (2001) Novel mechanism of wnt signalling inhibition mediated by dickkopf-1 interaction with lrp6/arrow. Nat Cell Biol. 3, 683-686
42 Hannoush, R. N. (2008) Kinetics of wnt-driven beta-catenin stabilization revealed by quantitative and temporal imaging. PLoS One. 3, e3498
43 Galli, L. M., Barnes, T., Cheng, T., Acosta, L., Anglade, A., Willert, K., Nusse, R. and Burrus, L. W. (2006) Differential inhibition of wnt-3a by sfrp-1, sfrp-2, and sfrp-3. Dev Dyn. 235, 681-690
44 Wawrzak, D., Metioui, M., Willems, E., Hendrickx, M., de Genst, E. and Leyns, L. (2007) Wnt3a binds to several sfrps in the nanomolar range. Biochem Biophys Res Commun. 357, 1119-1123
45 Tallarida, R. J. (2006) An overview of drug combination analysis with isobolograms. J Pharmacol Exp Ther. 319, 1-7
46 Bourhis, E., Tam, C., Franke, Y., Bazan, J. F., Ernst, J., Hwang, J., Costa, M., Cochran, A. G. and Hannoush, R. N. (2010) Reconstitution of a frizzled8.Wnt3a.Lrp6

signaling complex reveals multiple wnt and dkk1 binding sites on lrp6. J Biol Chem. 285, 9172-9179
47 Finch, P. W., He, X., Kelley, M. J., Uren, A., Schaudies, R. P., Popescu, N. C., Rudikoff, S., Aaronson, S. A., Varmus, H. E. and Rubin, J. S. (1997) Purification and molecular cloning of a secreted, frizzled-related antagonist of wnt action. Proc Natl Acad Sci U S A. 94, 6770-6775
48 Rulifson, E. J., Wu, C. H. and Nusse, R. (2000) Pathway specificity by the bifunctional receptor frizzled is determined by affinity for wingless. Mol Cell. 6, 117-126
49 Kholodenko, B. N., Demin, O. V., Moehren, G. and Hoek, J. B. (1999) Quantification of short term signaling by the epidermal growth factor receptor. J Biol Chem. 274, 30169-30181
50 Higashi, Y. and Sokawa, Y. (1982) Microinjection of interferon and 2',5'-oligoadenylate into mouse l cells and their effects on virus growth. J Biochem. 91, 2021-2028

Tables

Parameter name	***Value***	***Units***	***Reference***
k_1	*for sFRP1:* $4.33 \cdot 10^4$ *for sFRP2:* $11.4 \cdot 10^4$	$M^{-1} \cdot s^{-1}$	[44]
k_{-1}	*for sFRP1:* $4.86 \cdot 10^{-4}$ *for sFRP2:* $4.63 \cdot 10^{-4}$	s^{-1}	[44]
k_2	$7.9 \cdot 10^4$	$M^{-1} \cdot s^{-1}$	[44]
k_{-2}	$4.7 \cdot 10^{-4}$	s^{-1}	[44]
k_3	$2.8 \cdot 10^7$	$M^{-1} \cdot s^{-1}$	fitted
k_{-3}	0.1	s^{-1}	[49]
k_4	$1.03 \cdot 10^6$	$M^{-1} \cdot s^{-1}$	[41]
k_{-4}	$5.05 \cdot 10^{-4}$	s^{-1}	[41]
k_5	$5 \cdot 10^7$	$M^{-1} \cdot s^{-1}$	[19]
k_{-5}	10^{-4}	s^{-1}	[38]
k_6	$1.58 \cdot 10^8$	$M^{-1} \cdot s^{-1}$	fitted
k_{-6}	1.75	s^{-1}	[19]
k_7	$7 \cdot 10^{-12}$	$M^{-1} \cdot s^{-1}$	[19]
k_8	$4.2 \cdot 10^{-6}$	s^{-1}	[19]
F_T	30	*receptor/cell*	fitted
L_T	$4 \cdot 10^3$	*receptor/cell*	[41]
C_T	$2 \cdot 10^{-11}$	*M*	[19]
V_{cell}	3.5·10-13	*l*	[50]
W_T	*Determined by experimental conditions*	*M*	
S_T		*M*	
L_T		*receptor/cell*	
V_{exp}		*l*	
N_{cell}		*cell*	
λ	$4.88 \cdot 10^6$	*measurement units/M*	fitted*

Table 1. The model parameters. Parameter values were estimated directly from literature or found by fitting to experimental data, as specified in the rightmost column. The parameter interpretations are detailed in Materials and Methods section 1b.

*The value of λ characterizes the experimental system; its specific value for any system is determined by scaling the measurement units to those used in the experiment by which the model was calibrated.

Wnt3a [nM]	*β-catenin accumulation (%)*	*Combinations of sFRP1, Dkk1 [nM]*					*sFRP1/Dkk1 ratio*	
		a	***b***	***c***	***d***	***e***	*for e/ a*	*for c*
0.5	**5**	0, 33.6	11.8, 16.8	28.3, 8.6	54.3, 3.7	110.8, 0	3.3	3.3
0.5	**10**	0, 15.8	9.9, 7.9	17.9, 4.9	28.3, 2.8	57.6, 0	3.6	3.6
0.5	**20**	0, 7.2	7.5, 3.6	9.7, 2.9	14.1, 1.9	28.8, 0	4.0	3.4
0.5	**30**	0, 4.2	5.9, 2.1	8.6, 1.5	9.1, 1.4	18.6, 0	4.4	5.9
0.5	**40**	0, 2.8	4.8, 1.4	5.4, 1.2	6.5, 1.0	13.3, 0	4.8	4.4
0.5	**50**	0, 1.9	3.7, 0.9	3.9, 0.9	4.7, 0.7	9.5, 0	5.1	4.4
1	**10**	0, 16.8	11.4, 8.4	20.2, 5.3	35.1, 2.7	71.7, 0	4.3	3.8
2	**10**	0, 22.6	14.4, 11.3	32.5, 5.9	58.8, 2.7	119.9, 0	5.3	5.5
2.5	**10**	0, 25.4	15.9, 12.7	38.8, 6.1	70.3, 2.8	143.3, 0	5.6	6.3
4	**10**	0, 32.3	20.2, 16.1	51.2, 7.6	106.5, 2.9	217.2, 0	6.7	6.7
5	**10**	0, 36.3	22.3, 18.2	60.0, 8.2	132.4, 2.9	270.1, 0	7.4	7.3

Table 2. Simulated combinations of sFRP1 and Dkk1 yielding inhibition of β-catenin accumulation to specific levels. For each Wnt3a concentration and β-catenin accumulation level, five different combinations of sFRP1 and Dkk1 are suggested. Each row contains five points on one of the isoboles shown in Figs. 8C,D, e.g. the values in the grey (second) row correspond to the points marked ***a*** to ***e*** in Fig. 8D. These points are chosen as follows: in column ***a*** – Dkk1 alone; ***e*** – sFRP1 alone; ***b*** – half of the maximal Dkk1 concentration (specified in ***a***) and corresponding sFRP1 concentration; ***d*** – half of the maximal sFRP1 concentration (specified in ***e***) and corresponding Dkk1 concentration; ***c*** – maximally synergistic combination of sFRP1 and Dkk1 doses (see Materials and Methods). The last column presents the ratio between sFRP1 and Dkk1 concentrations in column ***c***, and the column next leftward to it presents the potency ratio (between sFRP1 in column ***e*** and Dkk1 in column ***a***).

Figures

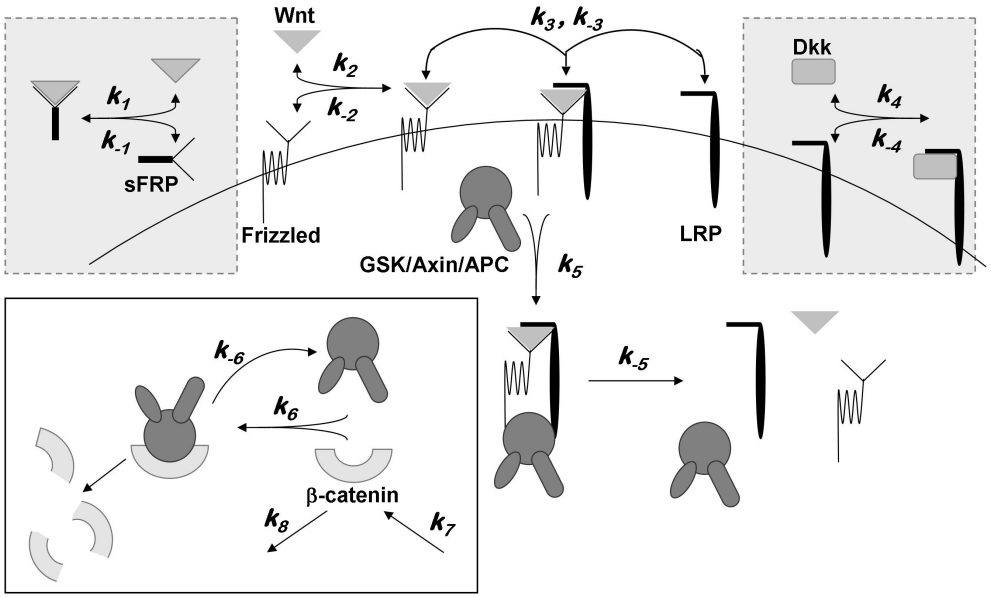

Figure 1. A schematic description of the mathematical model for the Wnt signaling pathway. The scheme shows the modeled reactions, indexed 1 to 8, as follows: (1) interaction between sFRP and Wnt ligand, (2) interaction between Wnt and Frizzled receptor, (3) interaction between Wnt-Frizzled complex and LRP, (4) interaction between Dkk and LRP, (5) interaction between ternary complex (Frizzled /Wnt/LRP) and destruction complex (GSK/Axin/APC), (6) interaction between β-catenin and destruction complex, (7) production of β-catenin, and (8) degradation of β-catenin, independent of destruction complex; forward and backward rate constants are indexed accordingly. The central part depicts the reactions transducing the signal from Wnt to the destruction complex, the grey parts show reactions between inhibitors and relevant pathway components, and the boxed part shows β-catenin regulation by the destruction complex.

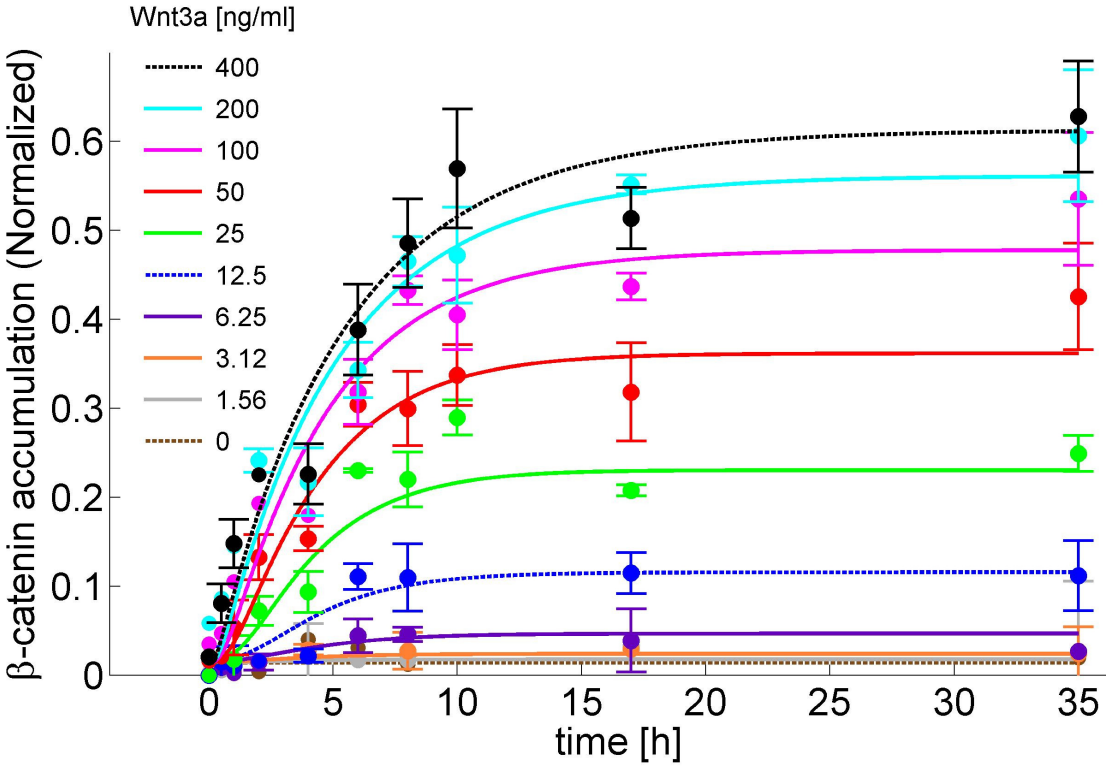

Figure 2. Model simulation of Wnt effect on β-catenin accumulation, compared to experimental data. Four of the model parameters were adjusted using partial training set, containing measurements of β-catenin accumulation under three Wnt3a concentrations (0, 12.5 and 400*ng/ml*). The model was then simulated, using the resulted parameter set, under all experimental Wnt3a concentrations, and simulation results were compared to the complete data. Circles represent averages (with s.e.m. bars, whenever available) from two independent experiments, each carried out in quadruplicate [42]. Dashed and solid lines are results of model simulations of partial training set data and all other Wnt3a concentrations, respectively. Points and lines in different colors correspond to different Wnt3a concentrations.

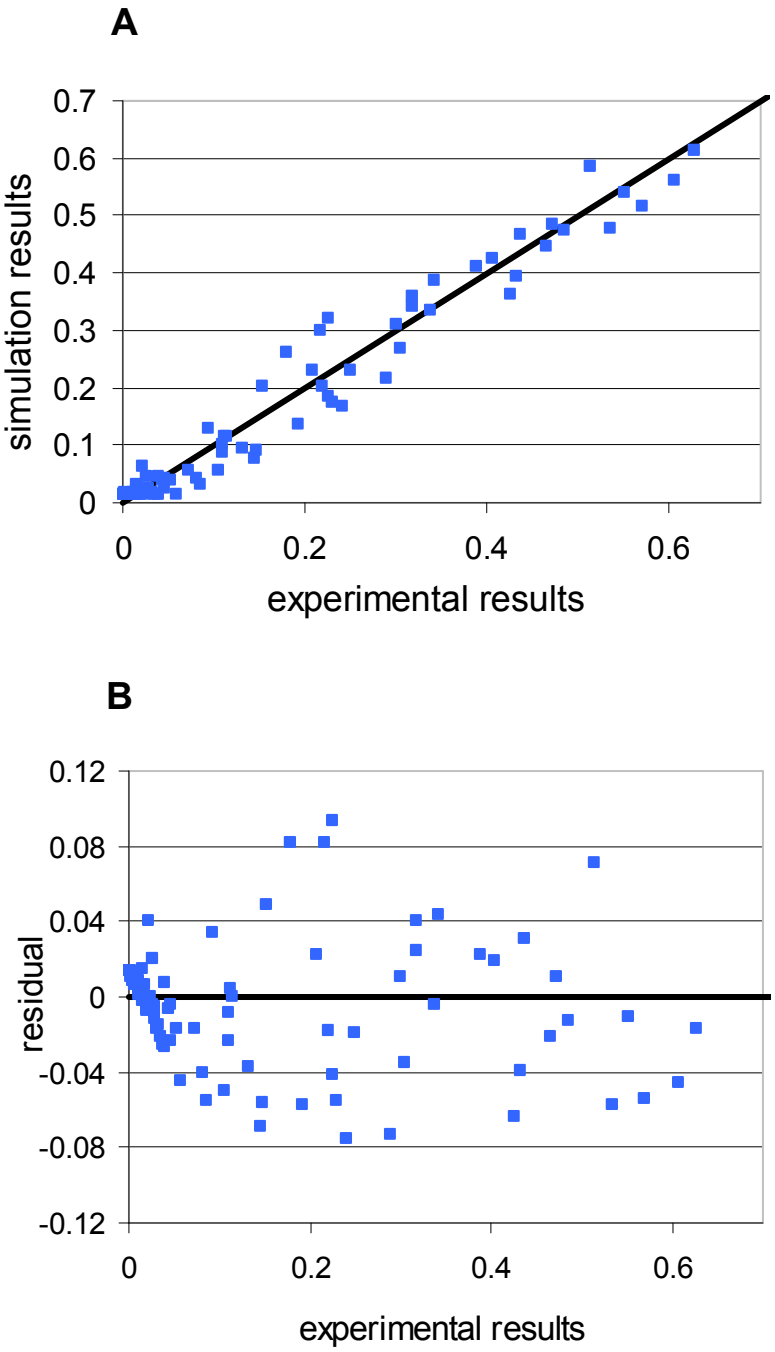

Figure 3. Statistical tests for the best-predictive parameter set: observed vs. predicted. (A) Simulation results vs. experimental results (B) Residues vs. experimental results. All axes units are normalized β-catenin units, as reported for the experiment [42].

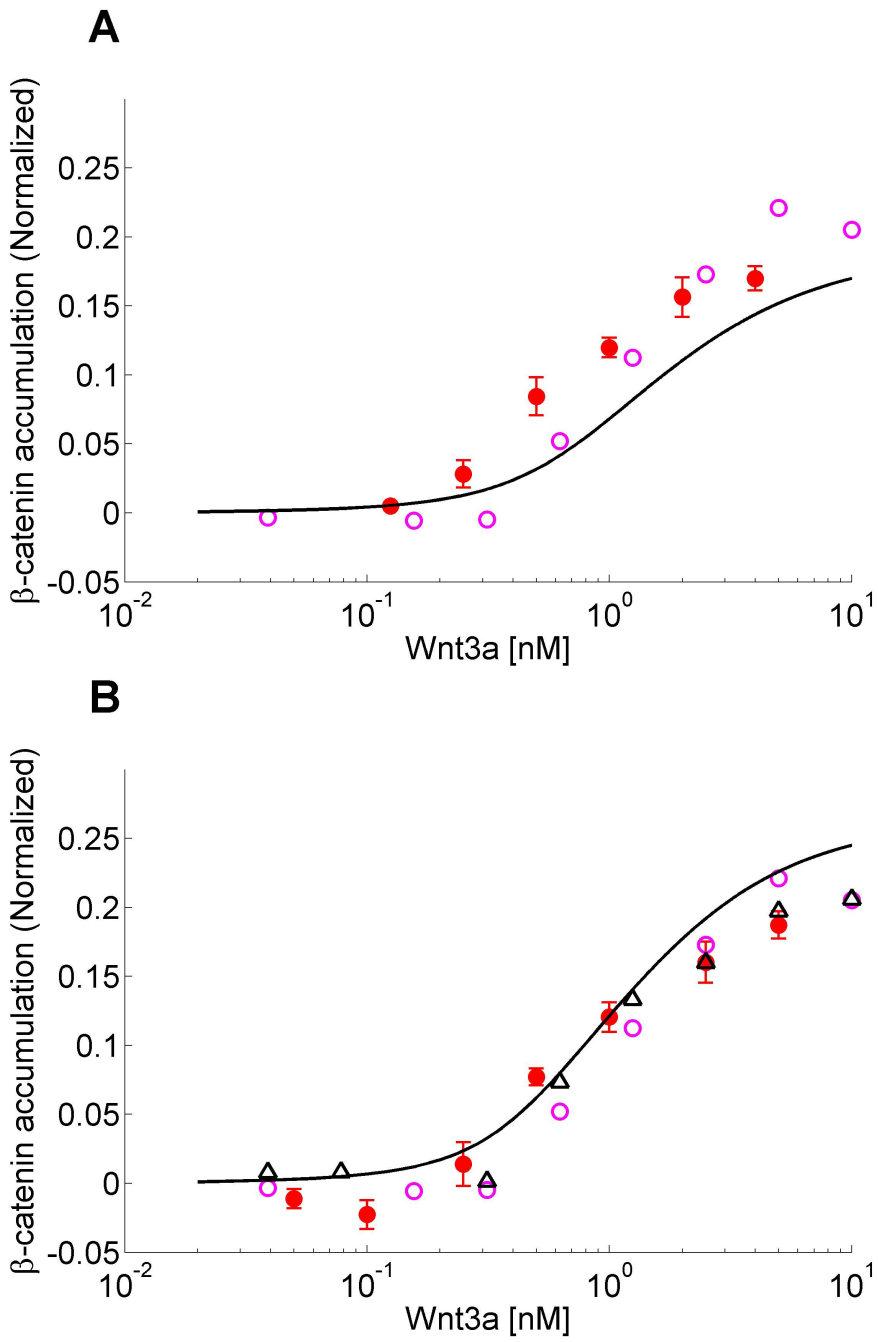

Figure 4. Model predictions of Wnt3a effect on β-catenin accumulation, compared to different experimental sources. (A) β-catenin accumulation after 2 hours, in the presence of different Wnt3a concentrations. Scaled data from [44] (red full circles) showing means and s.e.m. of 3 or 4 experiments, are presented along with model predictions (black line) and with average data from [42] (pink open circles). (B) Scaled data from [43] (red full circles) showing means and s.e.m. of 3 to 6 independent replicates, are presented along with model predictions (black line), for t=3 hours. No data for t=3 hours are available in [42]. For comparison we show data for t=2 hours (pink open circles), and for t=4 hours (black triangles) from there.

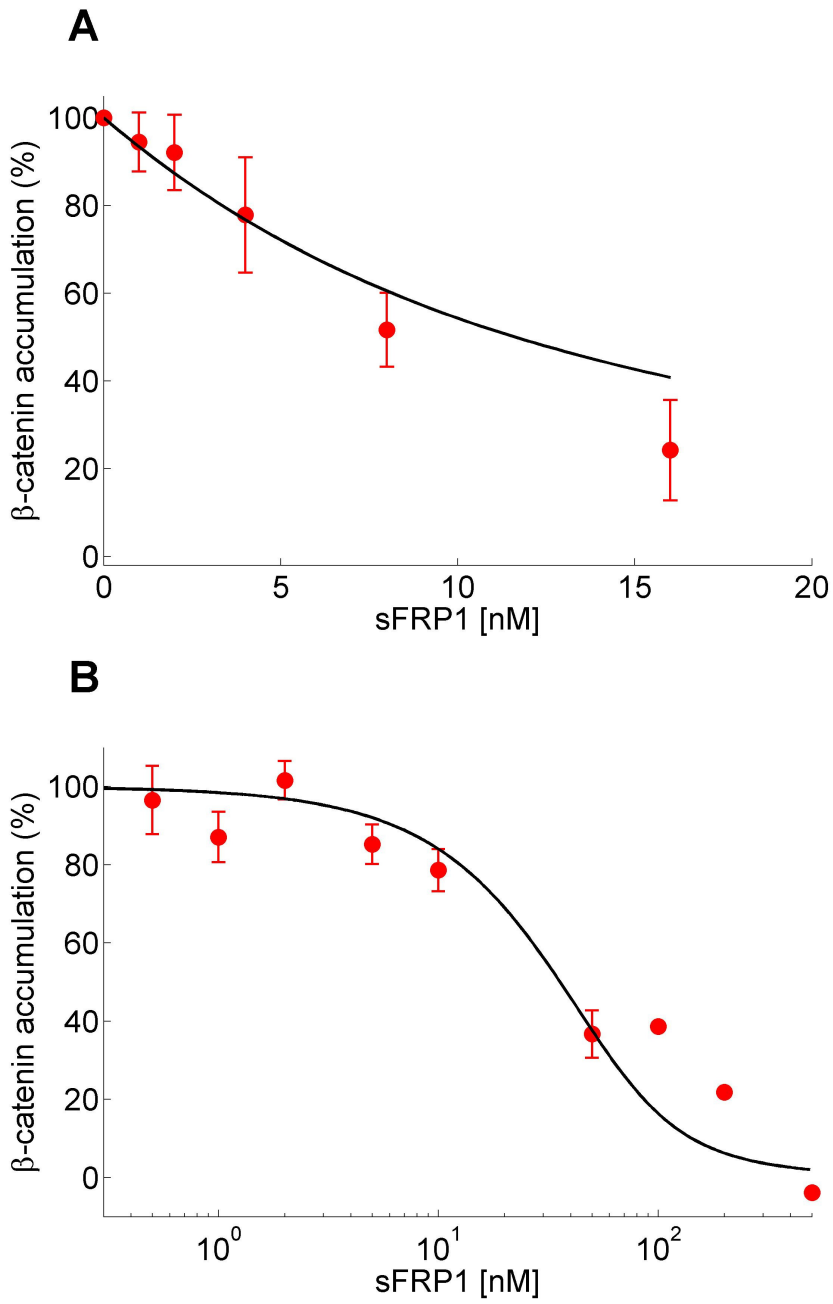

Figure 5. Model predictions of sFRP1 effect on β-catenin accumulation, compared to experimental results. (A) β-catenin inhibition as a function of sFRP1 concentration (means of 3 or 4 experiments with s.e.m. bars), as reported in [44] (red circles), along with model predictions for the same experiment (black line). (B) Similar comparison between means of 3 independent replicates reported by [43] (red circles), and model predictions (black line). The s.e.m. bars are shown whenever available. In accordance with the experiments setup, Wnt3a concentration is 0.5 and 2.5 *nM*, and β-catenin is sampled at t=2 and t=3 hours in (A) and (B), respectively. β-catenin accumulation is relative to maximal level (with Wnt3a only) and to base level (no Wnt3a).

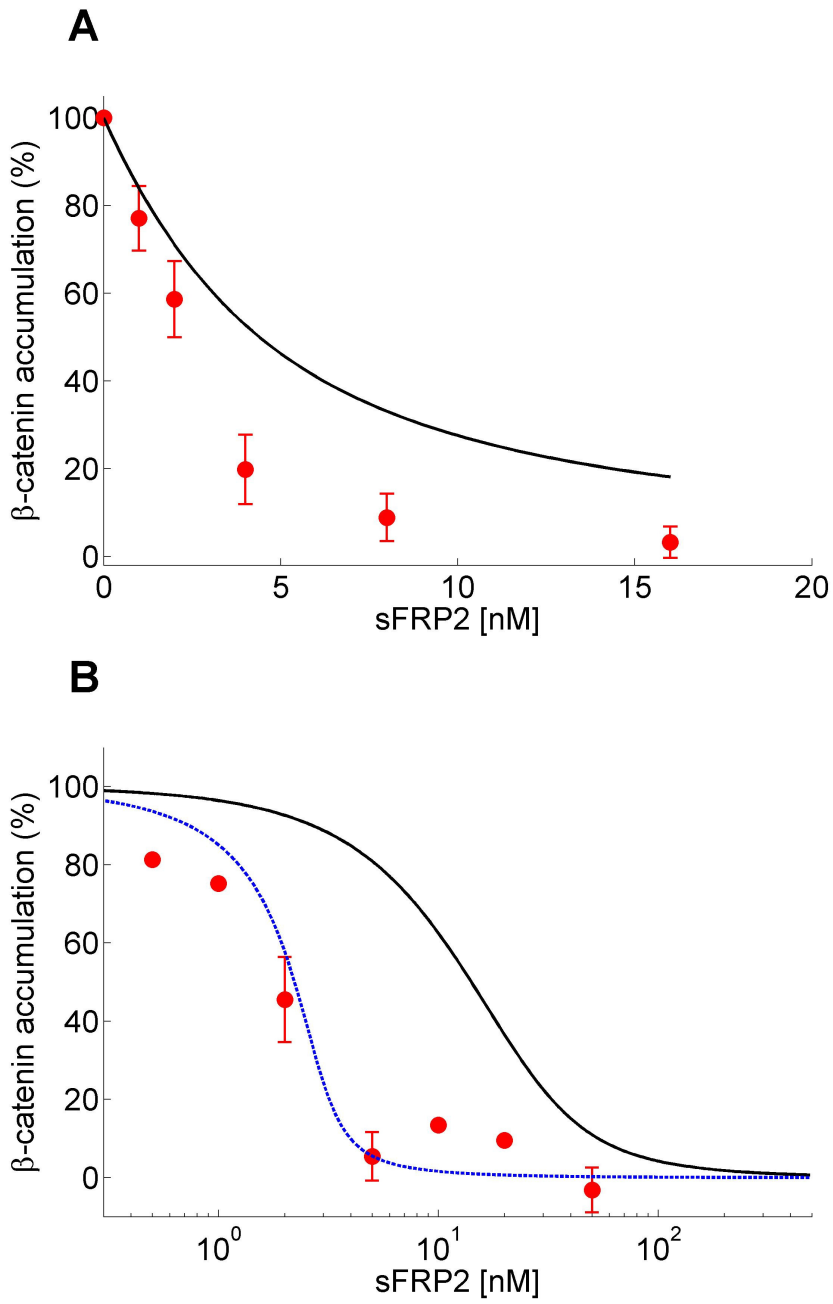

Figure 6. Model predictions of sFRP2 effect on β-catenin accumulation, compared to experimental results. (A) β-catenin inhibition as a function of sFRP2 concentration (means of 3 or 4 experiments with s.e.m. bars), as reported in [44] (red circles), along with model predictions for the same experiment (black line). (B) A similar comparison between means of 3 independent replicates from [43] (red circles) and predictions of the model before (solid black line) and after (dashed blue line) adjusting of Wnt3a-sFRP2 binding reaction rates. The s.e.m. bars are shown whenever available. In accordance with the experiments setup, Wnt3a concentration is 0.5 and 2.5 *nM*, and β-catenin is sampled at t=2 and t=3 hours in (A) and (B), respectively. Accumulation of β-catenin is relative to maximal level (with Wnt3a only) and to base level (no Wnt3a).

A

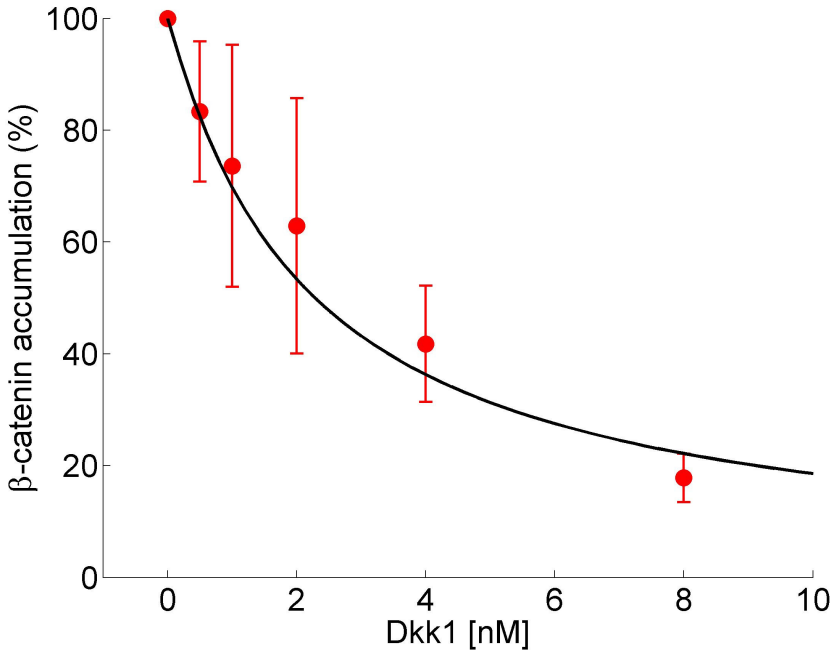

B

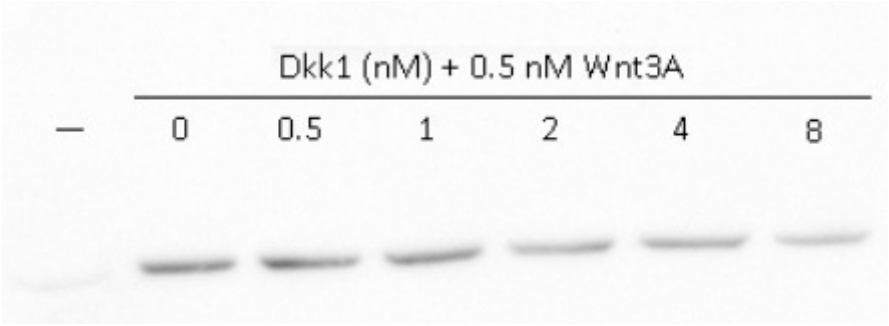

Figure 7. Inhibition of β-catenin accumulation by Dkk1 – prospectively validated model predictions. (A) The effect of Dkk1 on Wnt3a-induced β-catenin accumulation, as predicted by the model (black line) and experimentally tested thereafter (red circles). L cells were treated for two hours with 0.5 *nM* Wnt3a in combination with increasing concentrations of Dkk1. Average and s.e.m. of 3 independent experiments are shown. β-catenin accumulation is relative to maximal level (with Wnt3a only) and to base level (no Wnt3a). (B) Experimental β-catenin accumulation shown in a representative Western blot.

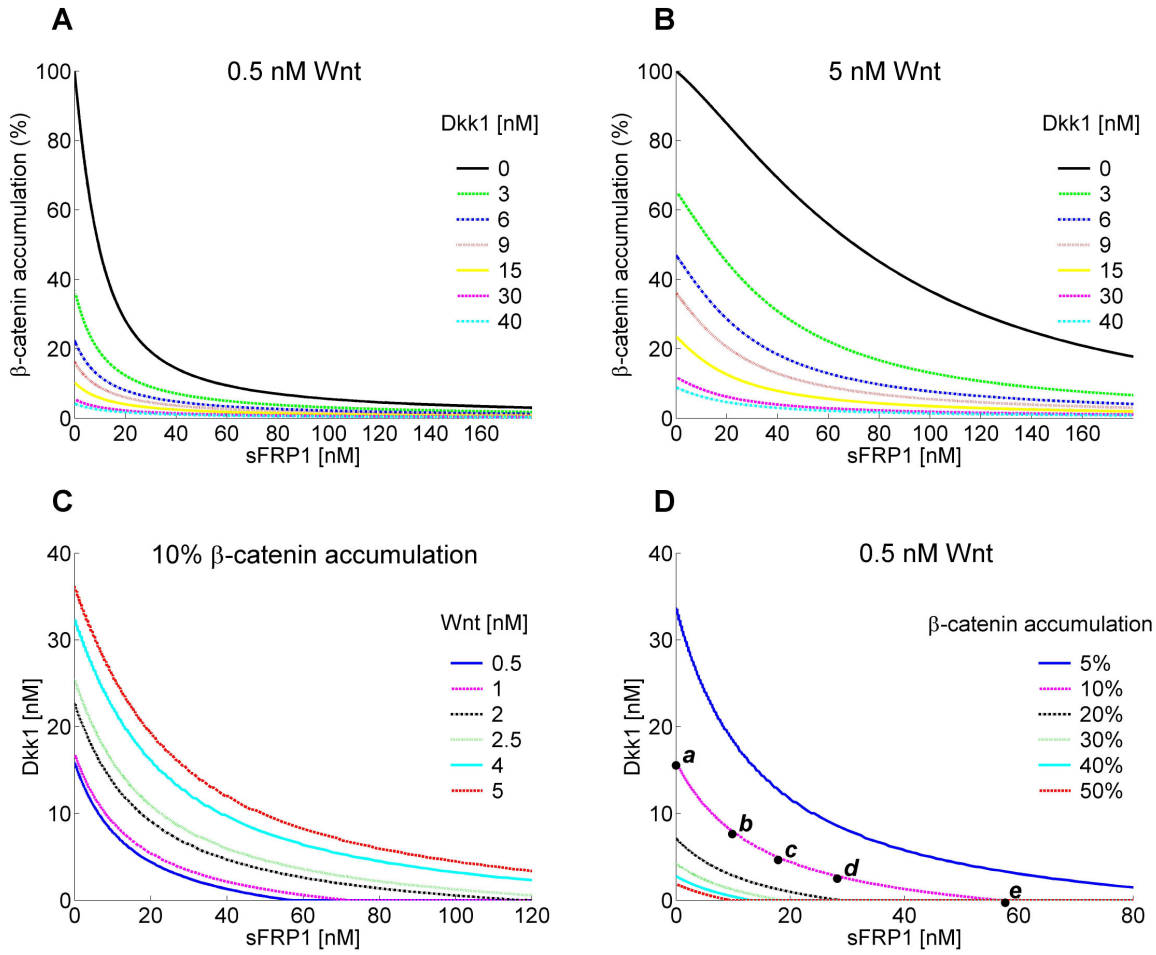

Figure 8. Combined effect of sFRP1 and Dkk1, predicted by the model. (A-B) β-catenin accumulation as a function of sFRP1 at different Dkk1 concentrations. Wnt3a concentration was set to 0.5 and 5 *nM* in (A) and (B), respectively. β-catenin accumulation units are relative to maximal level (with Wnt only) and to base level (no Wnt). (C-D) Isobolograms (graphs of isoboles) for the combined effect of Dkk1 and sFRP1. Each curve represents all combinations of sFRP1 and Dkk1 that inhibit β-catenin accumulation to a fixed level, in the presence of a given Wnt3a concentration. Panel (C) shows isoboles for β-catenin inhibition to 10% of the maximal level. Different curves correspond to different concentrations of Wnt3a. In panel (D), isoboles are shown for different fixed β-catenin accumulation levels, between 5% and 50% of the maximal level, obtained with 0.5 *nM* Wnt3a. Points ***a*** to ***e*** correspond to the values in the second line of Table 2. In all figures, β-catenin is sampled at t=3 hours.